Volume 6, Issue 6, 2016, 1797 - 1804 ISSN 2069-5837

Biointerface Research in Applied Chemistry

www. BiointerfaceResearch. com

Original Research Article Open Access Journal

Received: 01.11.2016 / Revised: 28.11.2016 / Accepted: 05.12.2016 / Published on-line: 08.12.2016

Structure and properties of Ag_2S/Ag semiconductor/metal heteronanostructure

Stanislav I. Sadovnikov [1,*], Aleksandr I. Gusev [1]

[1] Institute of Solid State Chemistry, Ural Branch of the Russian Academy of Sciences, Ekaterinburg 620990, Russia

*Corresponding author e-mail: ***sadovnikov@ihim.uran.ru***

ABSTRACT

Ag_2S/Ag heteronanostructure has been produced by a simple one-stage chemical deposition from aqueous solutions of silver nitrate, sodium sulfide, and sodium citrate with the use of monochromatic light irradiation. For simultaneous synthesis of Ag_2S and Ag nanoparticles, deposition has been performed from reaction mixtures with reduced sodium sulfide concentration. The formation of Ag_2S/Ag nanocomposite structures is confirmed by X-ray analysis, high-resolution electron microscopy, energy dispersion analysis and dynamic light scattering methods. It is established that in the contact layer between silver sulfide and silver, nonconducting α-Ag_2S acanthite transforms into superionic β-Ag_2S argentite under the action of external electric field. The scheme of the operation of a resistive switch based on an Ag_2S/Ag heteronanostructure is proposed.

Keywords: *silver sulfide; silver; heteronanostructure; acanthite-argentite phase transformation; resistive switch.*

1. INTRODUCTION

One of the most requisite semiconducting sulfides is the well known silver sulfide Ag_2S.

As early as in 1833, Faraday found that lead fluoride and silver sulfide possessed high ion conductivity comparable to the conductivity of metals in a wide temperature range [1]. He wrote: "I formerly described a substance, sulfuret of silver, whose conducting power was increased by heat. . . When a piece of that substance, which had been fused and cooled, was introduced into the circuit of a voltaic battery, it stopped the current. Being heated, it acquired conducting powers…" [2].

Unique chemical, structural, optical and conductive properties make silver sulfide an excellent substance for preparation of heterostructures.

Among composite heterostructures of silver sulfide, the semiconductor/metal heteronanostructure Ag_2S/Ag attracts special attention. It can be used in resistive switches and nonvolatile memory devices [3-6]. The action of the switch is based on the phase transformation between nonconducting α-Ag_2S acanthite and superionic β-Ag_2S argentite. According to the phase diagram of the system Ag – S [7], silver sulfide Ag_2S has three basic polymorphic modifications]. Low-temperature semiconducting phase α-Ag_2S (acanthite) with monoclinic crystal structure exists at temperatures below ~450 K. Monoclinic acanthite has a direct band gap of 0. 9-1. 05 eV. Under equilibrium conditions, cubic phase β-Ag_2S (argentite) exists in the temperature range 452–859 K and has a superionic conductivity. High-temperature face centered cubic (fcc) phase γ-Ag_2S stable from ~860 K up to melting temperature.

Known methods for the preparation of a heteronanostructures of Ag_2S or Ag mainly deal with the synthesis of nanoparticles of one species with the subsequent growth of other species nanoparticles [8-12]. These methods are rather expensive and time-consuming.

Chemical deposition is a promising route for preparing nanostructured semiconducting nanoparticles [13-17], thin-film structures and heteronanostructures [9,18]. By varying the concentration of reagents it is possible to change the number of sulfide phase nuclei in the initial moment of deposition and their growth rate. Thanks to this and different duration of deposition, sulfide particles with controllable size can be obtained. However the preparation of sulfide nanostructures from colloidal solutions is studied insufficiently and the conditions of synthesis as a rule are determined empirically.

Present paper is devoted to study of synthesis conditions of Ag_2S/Ag heteronanostructures by hydrochemical deposition method and determination of their structural characteristics. Present work is a continuation of a cycle of systematic studies of nanostructured silver sulfide [16, 17, 19-23] beginning with synthesis conditions, crystal structure, size and morphology of nanoparticles and ending with phase transformations and thermal properties of nanostructured Ag_2S.

2. EXPERIMENTAL SECTION

Ag_2S/Ag heteronanostructures have been synthesized by chemical deposition from aqueous solutions of $AgNO_3$, Na_2S, and $Na_3C_6H_5O_7 \equiv Na_3Cit$ under light irradiation with reduced (as compared with expected silver sulfide stoichiometry) concentration of sodium sulfide (Table 1). Earlier nanocrystalline Ag_2S sulfide has been synthesized by the same method but without photoirradiation [19]. For comparison, Ag_2S nanoparticles without an impurity of metallic Ag have been synthesized in the dark from reaction mixture with small excess of Na_2S, i. e., $C_{Na_2S} = (C_{AgNO_3}/2) + \delta$ $C_{Na_2S} = (C_{AgNO_3}/2) + \delta$ where $\delta = 0.5$ mmol·l^{-1} (*see* Table 1).

Table 1. Composition of the reaction mixtures, average particle size D_{aver} and content of silver sulfide Ag_2S and Ag in the Ag_2S/Ag heteronanostructures

No.	Concentration of reagents in the reaction mixture (mmol·l^{-1})			D_{aver} (nm) in deposited powders		D_{aver} (nm) in colloidal solutions				Content of Ag_2S and Ag in Ag_2S/Ag heteronanostructures			
						Ag_2S		Ag		Ag_2S		Ag	
	$AgNO_3$	Na_2S	Na_3Cit	BET [2]	XRD [3]	DLS	TEM	DLS	TEM	C [4] (wt. %)	N [5] (%)	C [4] (wt. %)	N [5] (%)
1	50	25-δ [1]	100	56	48±6	28±6	36	9±2	12	95. 0	68	5. 0	32
2	50	25-δ [1]	25	84	52±8	32±6	38	14±3	15	92. 5	61	7. 5	39
3	50	25-δ [1]	12. 5	56	46±6	34±6	42	11±3	16	98. 0	56	2. 0	44
4	50	25+δ [1]	10	-	55±6	18±5	35	-	-	100. 0	100. 0	0	0

[1] δ = 0. 5 mmol·l^{-1} (small deficiency of Na_2S is necessary for the synthesis of Ag_2S/Ag heteronanostructures, small excess of Na_2S is necessary for synthesis of Ag_2S nanoparticles without an impurity of metallic Ag);
[2] average size D_{aver} of Ag_2S/Ag nanocomposite particles;
[3] average size D_{aver} of Ag_2S nanoparticles;
[4] C is weight content of Ag_2S and Ag;
[5] N is relative number of Ag_2S and Ag nanoparticles.

All the Ag_2S/Ag heteronanostructures were examined by XRD method on a Shimadzu XRD-7000 and STADI-P (STOE) diffractometers in Cu$K\alpha_1$ radiation. The XRD measurements were performed in the angle interval 2θ = 20-95° with a step of $\Delta(2\theta)$ = 0. 02° and scanning time of 10 sec in each point. The determination of the crystal lattice parameters and final refinement of the structure of synthesized heteronanostructures were carried out with the use of the X'Pert HighScore Plus software package [24].

The average particle size D (to be more precise, the average size of coherent scattering regions (CSR)) in deposited silver sulfide powders was estimated by XRD method from the diffraction reflection broadening using the dependence of reduced reflection broadening $\beta^*(2\theta) = [\beta(2\theta)\cos\theta]/\lambda$ on the scattering vector $s = (2\sin\theta)/\lambda$ [15,25]. The value of broadening $\beta(2\theta)$ was determined by comparing the experimental width of each diffraction reflection, $FWHM_{exp}$, with the instrumental resolution function $FWHM_R$ of the X-ray diffractometer as $\beta(2\theta) = [(FWHM_{exp})^2 - (FWHM_R)^2]^{1/2}$. The resolution function $FWHM_R(2\theta) = (u\tan^2\theta + v\tan\theta + w)^{1/2}$ of the Shimadzu XRD-7000 diffractometer was determined in a special diffraction experiment using the cubic lanthanum hexaboride LaB_6 (NIST Standart Reference Powder 660a) with lattice constant a = 0. 41569162 nm. The parameters of this resolution function $FWHM_R(2\theta)$ are u = 0. 00616, v = -0. 00457, and w = 0. 00778.

The Ag_2S/Ag heteronanostructures were examined by high-resolution transmission electron microscopy (HRTEM) method also. The HRTEM images were recorded on a JEOL JEM-2010 transmission electron microscope with 140 pm (1. 4 Å) lattice resolution. The elemental chemical composition of all the types of nanostructured silver sulfide was studied on the same microscope with the use of an Phoenix (EDAX) Energy Dispersive Spectrometer with a Si(Li) detector having energy resolution of 130 eV. For examination, colloidal solutions of Ag_2S nanoparticles were placed on a copper grid with collodium-glue covering. One or two layers of collodium-glue (alcoholic solution of kolloksilin) were applied to Cu grid. After the drying of the glue coating, a carbon-containing grid with voids is formed.

The microstructure, size and elemental chemical composition of Ag_2S/Ag heteronanostructures were studied by the scanning electron microscopy (SEM) method on a JEOL-JSM LA 6390 microscope coupled with a JED 2300 Energy Dispersive X-ray Analyzer.

The average particle size D was also estimated from the value of specific surface area S_{sp}. The specific surface area S_{sp} of the synthesized silver sulfide powders was found by the Brunauer-Emmett-Teller (BET) method from the isotherms of low-temperature adsorption of molecular nitrogen vapors at 77 K. The measurements were carried out by means of a Gemini VII 2390t Surface Area Analyzer. In the approximation that all particles have similar size and spherical shape, the average particle size D is equal to $6/\rho S_{sp}$ (ρ = 7. 25 g·cm^{-3} is the density of silver sulfide).

The size (hydrodynamic diameter) D_{dls} of the nanoparticles in the colloidal solutions was determined by non-invasive Dynamic Light Scattering (DLS) on a Zetasizer Nano ZS facility (Malvern Instruments Ltd) at 298 K. The He-Ne laser wavelength was 633 nm, the detection angle of back-scattering light was 173°. To provide reproducibility of the results, light scattering and particle size in each solution were measured minimum 3 times. Treatment of measurement results of particle size distribution was performed using multiple narrow modes with high resolution.

3. RESULTS AND DISCUSSION

In the reaction mixtures with reduced concentration of Na_2S, along with the formation of Ag_2S sulfide, silver Ag nanoparticles are deposited. Controlling the synthesis conditions, Ag_2S/Ag heteronanostructures can be produced with different ratio of Ag and Ag_2S nanoparticle sizes. Synthesis was carried out in the following sequence: a complexing agent was added to silver nitrate in the dark; then a solution of Na_2S was poured into the

prepared solution (Fig. 1(*a*)). As a result, deposition of silver sulfide occurred by the following reaction

$$2AgNO_3 + Na_2S \xrightarrow{Na_3C_6H_5O_7} Ag_2S\downarrow + 2NaNO_3. \quad (1)$$

Further the solution was irradiated with monochromatic light with wavelength 450 nm. In accordance with photochemical reaction,

$$C_6H_5O_7^{3-} + 2Ag^+ \xrightarrow{\lambda} C_5H_4O_5^{2-} + CO_2 + H^+ + 2Ag\downarrow, \quad (2)$$

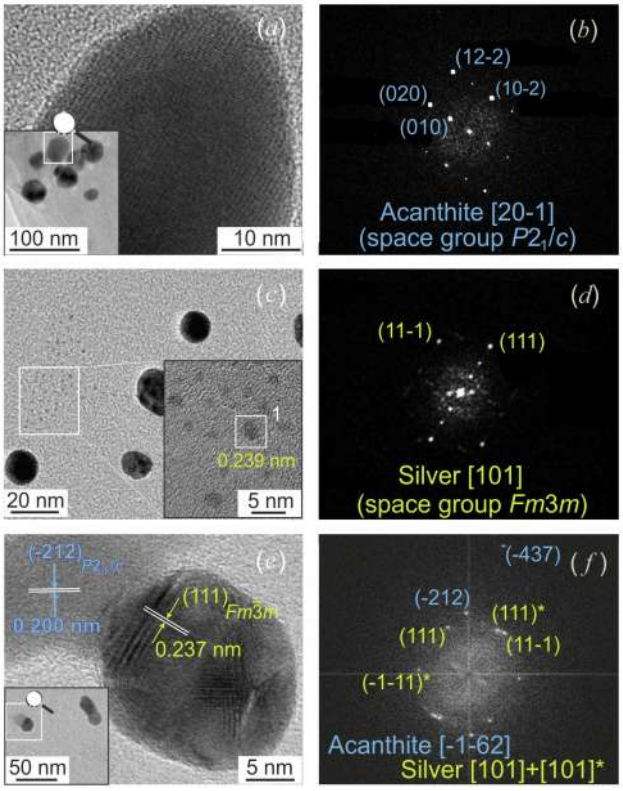

Figure 1. TEM and HRTEM images of (*a*) Ag_2S nanoparticles, (*c*) Ag nanoparticles, and (*e*) Ag_2S/Ag heteronanostructures, and FFT patterns (*b*), (*d*), and (*f*) obtained from the (*a*), (*c*), and (*e*) HRTEM images, respectively.

The citrate ions $C_6H_5O_7^{3-}$ reduce the Ag^+ ions to Ag nanoparticles in aqueous solutions and transform into acetone-1,3-dicarboxylate ions $C_5H_4O_5^{2-}$. The reduction of silver at the surface of Ag_2S nanoparticles leads to the formation of the Ag_2S/Ag heteronanostructures.

Sodium citrate plays a triple role in synthesis of Ag_2S/Ag heteronanostructures. Firstly, it is a complexing and stabilizing agent during deposition of Ag_2S sulfide nanoparticles. Secondly, during deposition in the light sodium citrate reduce the Ag^+ ions to metallic silver nanoparticles. Thirdly, citrate is absorbed on nanoparticles and prevents their agglomeration.

TEM and HRTEM images of Ag_2S, Ag and Ag_2S/Ag particles and their diffraction patterns are shown in Fig. 1.

The diffraction patterns (Fig. 1(*b*), 1(*d*), and 1(*f*)) of these particles are obtained by Fast Fourier Transformation (FFT) of their HRTEM images. The observed set (Fig. 1*b*) of diffraction reflections and interplanar distances of silver sulfide nanoparticle corresponds to monoclinic (space group $P2_1/c$) nanocrystalline acanthite α-$Ag_{1.\ 93}S$ [19]. The Ag nanoparticle with cubic (space group $Fm\bar{3}m$) structure clearly exhibits microtwinning in the direction of the [111] planes. The performed FFT of the HRTEM image of silver nanoparticle confirms the observed twinning (Fig. 1*d*). Diffraction (Fig. 1*f*) obtained by FFT of HRTEM image (Fig. 1*e*) of Ag_2S/Ag heteronanostructure revealed reflections of monoclinic silver sulfide and twinned reflections of cubic silver.

According to the EDX results, the content of silver Ag and sulfur S in Ag_2S nanoparticle is equal ~86. 3±0. 4 and ~12. 9±0. 1 wt. % and corresponds to ~$Ag_{1.\ 95\text{-}1.\ 98}S$ sulfide. Ag nanoparticle contains silver only, and Ag_2S/Ag heteronanostructure which is shown in Fig. 1(*e*) contains about 87. 8 and 11. 5 wt. % of Ag and S, respectively.

The XRD pattern of Ag_2S/Ag heteronanostructure produced from reaction mixture 2 is shown in Fig. 2*a*. The heteronanostructure contain two phases – monoclinic silver sulfide with α-Ag_2S acanthite structure and metallic cubic silver Ag. Detailed XRD studies of the crystal structure of α-Ag_2S acanthite and β-Ag_2S argentite phases were performed earlier in our works [16, 19, 21, 22]. The quantitative analysis of the XRD pattern (Fig. 2*a*) and comparison with data [19] have shown that the observed set of diffraction reflections corresponds to nanocrystalline nonstoichiometric monoclinic (space group $P2_1/c$) acanthite α-$Ag_{1.\ 93}S$ and cubic (space group $Fm\bar{3}m$) silver Ag. The crystallographic information file (CIF) for cubic (space group $Im\bar{3}m$) argentite β-Ag_2S (CCDC reference number 1062400) is presented in our study [21] as Electronic Supplementary Information (*see* DOI: 10. 1039/c5cp02499d). The diffraction reflection broadening (*see* Fig. 2*a*) is indicative of the nanosized state of the both phases. The content of Ag and Ag_2S in the nanopowders deposited from reaction mixtures 1, 2, and 3 is equal to ~5. 0 and ~95. 0 wt. %, ~7. 5 and ~92. 5, and ~2. 0 and ~98. 0, respectively (*see* Table 1). For the electron microscopy study of the two-phase nanoparticles, we used the colloidal solutions above the deposited powders. The HRTEM image of Ag_2S/Ag heteronanostructure is shown in Fig. 2*b*. It is seen that the Ag_2S and Ag nanoparticles are in direct contact and form the heteronanostructure.

Crystal structure and interplanar distances were determined for single Ag_2S nanoparticles by HRTEM method. Selected area of electron diffraction was obtained by standard FFT of selected area of HRTEM image. Then we carried out inverse FFT of the selected diffraction reflections in the HRTEM image using the Gatan Microscopy Suite software [26], and determined the interplanar distances corresponding to these diffraction reflections. The scheme of sequence of operation for determination of the interplanar distances for the diffraction reflections, observed on SAED, is shown in Fig. 3. Detailed description of determination of interplanar distances with the use of the Gatan Microscopy software [26] is given on site [27].

In the examination of heteronanostructures, it is necessary to determine the crystallographic indices of reflections obtained experimentally by electron diffraction method or FFT of the HRTEM images. This is especially important for exact identification of phase components which form a heteronanostructure. For compounds with oblique-angled (triclinic and monoclinic) unit cells, errors are sometimes committed during reflection indexing. In particular, Xu *et al*. [4] incorrectly determined the diffraction reflection indices of monoclinic acanthite α-Ag_2S in Ag/Ag_2S/W heteronanostructure. Authors [28] incorrectly determined the indices of diffraction reflections and interplanar distances of metallic silver for Ag/polypyrrole

composite on Si substrate. Such errors can be found in many studies devoted to the Ag_2S/Ag heteronanostructures in which monoclinic (space group $P2_1/c$) α-Ag_2S acanthite, cubic (space group $Im\bar{3}m$) β-Ag_2S argentite with body centered cubic (bcc) crystal lattice, and cubic (space group $Fm\bar{3}m$) silver Ag can coexist. Usually, the electron diffraction indices (hkl) are determined by comparing the derived interplanar distances d_{hkl} with the d_{hkl} values corresponding to a unit cell with known parameters. The authors [4] compared their data on acanthite with stale data [29], according to which the unit cell of monoclinic (space group $P2_1/n$) acanthite α-Ag_2S has parameters a = 0. 423 nm, b = 0. 691 nm, c = 0. 787 nm and β = 99. 6°.

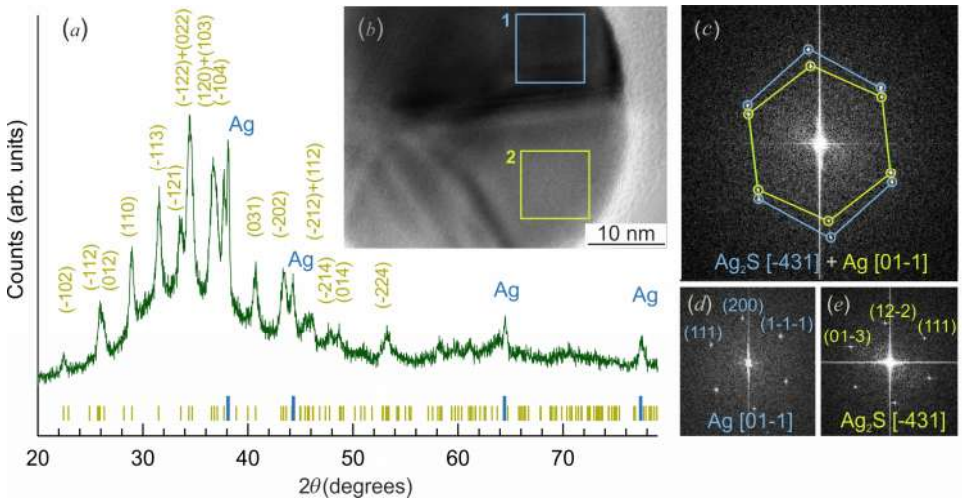

Figure 2. (*a*) XRD pattern and (*b*) HRTEM image of Ag_2S/Ag heteronanostructure. (*c*), (*d*), and (*e*) diffraction patterns obtained by FFT of HRTEM image of the whole composite heteronanostructure and its areas (1) and (2). The long and short ticks on XRD pattern correspond to reflections of cubic metallic Ag and monoclinic Ag_2S silver sulfide, respectively.

However, in low-symmetry structures, the neighbor values of d_{hkl} differ very slightly forming an almost continuous spectrum. That is why the error in determining the indices (hkl) of reflections from the value of d_{hkl} in low-symmetry structures is large. Much more accurately we can determine the angle φ_{refl} between the reflections with assumed indices ($h_ik_il_i$) on the FFT pattern, i. e. the angle between the straight lines passing through each reflection and the central spot (000).

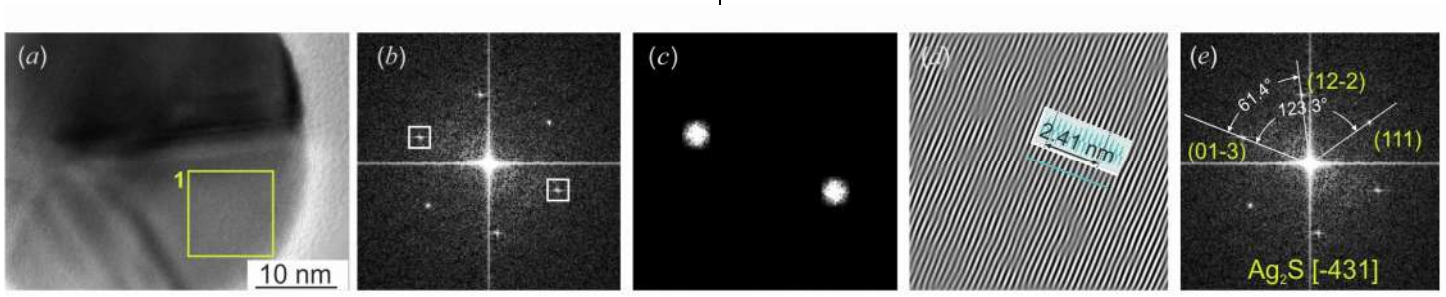

Figure 3. Sequence of operation for determination of the interplanar distances includes following steps: (*a*) uploading of HRTEM image in Gatan Microscopy Suite and selection of area in HRTEM image for FFT (green square); (*b*) creation of FFT from the selected area and selection of a spot on FFT; (*c*) creation of a mask from FTT; (*d*) creation of inverse FFT using mask, creation of line scale profile on FFT, and calculation of interplanar distance; (*e*) determination of (*hkl*) indices. Then steps *b*, *c*, *d*, and *e* are repeated for another spots.

To refine the derived indices, it is necessary to calculate the angles φ_{refl} between reflections with indices ($h_ik_il_i$) and compare them with the experimental angles between these reflections. The coincidence of the estimated and experimental φ_{refl} angles unequivocally proves that the indices ($h_ik_il_i$) are determined correctly.

In order to calculate the angles φ_{refl}, i. e. the angles between the atomic surface normals, it is necessary to transform the non-orthogonal (triclinic or monoclinic) coordinates into rectangular coordinates and then, using the transformed coordinates, to determine the basis vector of the reciprocal cell. For example, the basis vectors $(100)_{mon}$, $(010)_{mon}$ and $(001)_{mon}$ of the monoclinic unit cell written in rectangular coordinates have the form $\mathbf{a} = (a00)$, $\mathbf{b} = (0b0)$ and $\mathbf{c} = (c\cos\beta\ 0\ c\sin\beta)$, respectively. The basis vectors of the reciprocal lattice found by the known formula have the form $\mathbf{a^*} = (1/a\ 0\ -\cos\beta/(a\sin\beta))$, $\mathbf{b^*} = (0\ -1/b\ 0)$ and $\mathbf{c^*} = (0\ 0\ 1/(c\sin\beta))$. Accordingly, the arbitrary vector $(hkl)^*_{mon}$ $(hkl)^*_{mon}$ of the reciprocal lattice in the rectangular coordinate system has the explicit form

$$(hkl)^*_{mon} = h\mathbf{a}^* + k\mathbf{b}^* + l\mathbf{c}^* \equiv \left(\frac{h}{a} \quad -\frac{k}{b} \quad \frac{al - hc\cos\beta}{ac\sin\beta}\right) \qquad (3)$$

where $h_{cub} = h/a$, $k_{cub} = -k/b$ and $l_{cub} = (al - hc\cos\beta)/(ac\sin\beta)$.

The angle φ_{refl} between reflections ($h_1k_1l_1$) and ($h_2k_2l_2$) in the rectangular coordinate system is determined by the standard formula

$$\cos\varphi = \frac{h_{1cub}h_{2cub} + k_{1cub}k_{2cub} + l_{1cub}l_{2cub}}{\sqrt{h_{1cub}^2 + k_{1cub}^2 + l_{1cub}^2} \times \sqrt{h_{2cub}^2 + k_{2cub}^2 + l_{2cub}^2}} \quad (4)$$

Replacing in eq. (4) the cubic indices h_{cub}, k_{cub} and l_{cub} by their values expressed through monoclinic indices h, k and l, we obtain the formula for determining the angles φ_{refl} between the reflections $(h_1k_1l_1)_{mon}$ and $(h_2k_2l_2)_{mon}$ in the reciprocal lattice of monoclinic structure

$$\cos\varphi = \frac{h_1h_2/a^2 + k_1k_2/b^2}{d_1 \times d_2} + \\ + \frac{l_1l_2a^2 - (h_1l_2 + h_2l_1)ac\cos\beta + h_1h_2c^2\cos^2\beta}{(d_1 \times d_2)(ac\sin\beta)^2} \quad (5)$$

where $d_i = \sqrt{(h_i/a)^2 + (k_i/b)^2 + [(l_ia - h_ic\cos\beta)/(ac\sin\beta)]^2}$ with $i = 1$ or 2.

It is easily seen that expression (5) at $\beta = 90^\circ$ is transformed into a standard expression suitable for the description of structures with orthogonal (orthorhombic, tetragonal, cubic) unit cells.

As an example, at the top of Fig. 4 there is figure 2 borrowed from article [4] with a HRTEM image of monoclinic acanthite and an incorrect indexing of reflections on the FFT patterns obtained from regions (1) and (2) of this image. At the bottom of Fig. 4, correct indexing of the same reflections with allowance for the experimental values of angles φ_{refl} is shown.

For instance, in Fig. 4*d*1 the experimental angles between the hypothetical reflections (111) and (121) or between (121) and (010) are equal to ~27. 3° and ~56. 3° [4]. The angles between such reflections, which were estimated in study [4], should be 17. 8° and 45. 1° and they do not coincide with the experimental values. Consequently, the reflection indices are determined incorrectly. We have determined the indices of these reflections using region 1 on the HRTEM image (Fig. 4) in article [4]. These reflections have indices (11-2), (10-3) and (0-1-1), the calculated angles between them are equal to 27. 0° and 56. 6°, which coincides with the experimental values of φ_{refl} (Fig. 4*a*). The analysis showed that these reflections are observed along the [-31-1] zone axis rather than along [-101] as stated by Xu *et al* [4].

The indices of diffraction reflections of monoclinic acanthite α-Ag_2S on the FFT pattern (Figure 4*d*2) and other FFT patterns in study [4] are also determined incorrectly. In study [4], only the diffraction reflection indices of cubic (space group $Fm\bar{3}m$) silver Ag and cubic (space group $Im\bar{3}m$) argentite β-Ag_2S are determined correctly.

Note also that for analysis of the transformation of monoclinic acanthite into cubic argentite, the structure of acanthite would be more properly described in the space group $P2_1/c$ proposed in work [30] and refined for artificial coarse-crystalline acanthite in work [16] and for nanocrystalline acanthite in work [19].

In order to exclude the errors at experimental determination of angles φ_{refl}, an area of HRTEM image selected for FFT should have the square form. As an example, square area (*a*) of HRTEM image of monoclinic acanthite α-Ag_2S and FFT (*b*) of this image with indexing of observed diffraction spots and the experimental values of angles φ_{refl} are shown in Figure 5. The interplanar distances are determined by inverse FFT of the selected diffraction spots using the Gatan Misroscopy Suite software [26].

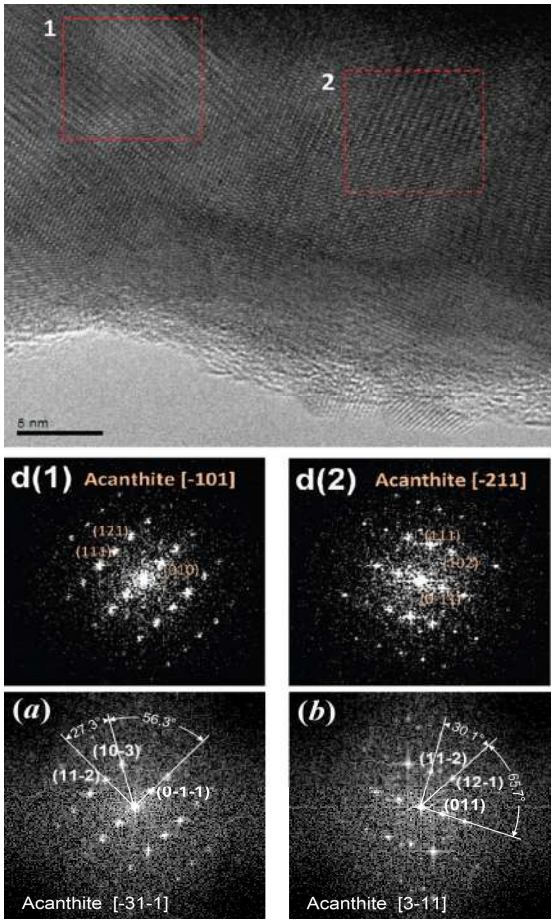

Figure 4. The HRTEM image of monoclinic acanthite from article [4] and indexing of reflections on the FFT patterns obtained from different regions (1) and (2) of this image: (*d*1) and (*d*2) are incorrect reflection indices reported in study [4]; (*a*) and (*b*) are correct reflection indices on the FFT patterns obtained from regions (1) and (2).

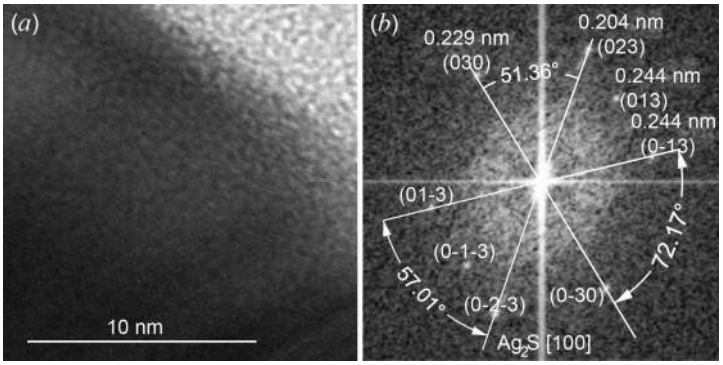

Figure 5. The HRTEM image (*a*) of monoclinic acanthite α-Ag_2S and FFT (*b*) of this image with indexing of observed diffraction spots and the experimental values of angles φ_{refl}.

The comparison of found interplanar distances 0,229, 0. 204, 0. 244, and 0. 244 nm (*see* Fig. 5*b*) with data [19] shown that the observed diffraction spots can have following crystallographic indices (030), (023), (013), and (0-13) of monoclinic (space group $P2_1/c$) acanthite.

As is seen, the experimental angles φ_{refl} between the hypothetical reflections (030) and (023) or between (023) and (0-13) are equal to ~51. 4° and ~57. 0° (Fig. 4*b*). The calculated angles φ_{refl} between these reflections should be 53. 3° and 57. 2° and they coincide with the experimental angles within the limits of

measurement errors. Analogously, the experimental angles φ_{refl} between the hypothetical reflections (013) and (0-13) or between (0-13) and (0-30) are equal to ~39. 5° and ~72. 2°. The calculated angles φ_{refl} between are equal 40. 9° and 69. 5° and coincide with the experimental angles. The analysis showed that these reflections are observed along the [100] zone axis of monoclinic (space group $P2_1/c$) acanthite α-Ag_2S.

In present study the indices (*hkl*) of the electron diffraction reflections have been determined with taking into account interplanar distances d_{hkl} and angles φ_{refl} between observed reflections.

HRTEM image of Ag_2S/Ag heteronanostructure produced from the reaction mixture 2 is shown in Fig. 2*b*. The diffraction pattern (*d*) obtained by FFT of HRTEM image of the whole this composite heteronanostructure contains two set of diffraction reflections corresponding to monoclinic silver sulfide and cubic silver. The diffraction patterns (*e*) and (*f*) are obtained by FFT from areas (1) and (2) isolated by green and orange quadrates. The observed set (*e*) of spots (111), (200), and (1-1-1) corresponds to the [01-1] plane of the reciprocal lattice of cubic Ag. The interplanar distances for area (2) and the set (*f*) of spots (01-3), (12-2), and (111) correspond to monoclinic α-Ag_2S acanthite. The DLS measurements of the particle size in colloidal solutions 1, 2, and 3 showed that the size and volume distributions are bimodal (Fig. 6).

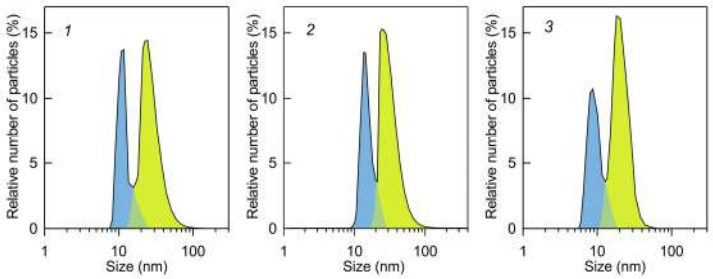

Figure 6. Bimodal size distributions of nanoparticles for colloidal solutions 1, 2, and 3. Maxima of distributions at ~7-15 nm correspond to Ag nanoparticles mainly, maxima of distributions in the region of 20-50 nm correspond to Ag_2S nanoparticles predominantly.

This means that these colloidal solutions contain two groups of particles – small particles and larger particles. Taking into consideration the TEM data for Ag_2S/Ag heteronanostructures, it can be supposed that small particles are Ag particles and larger particles are Ag_2S particles. Thus, the DLS measurements confirm indirectly the presence of Ag and Ag_2S particles in colloidal solutions 1, 2, and 3. The Ag particles are 2-3 times smaller in size than the Ag_2S particles. Therefore, the volume of individual Ag particle is ~10-20 times smaller than the volume of Ag_2S particle. Because of the small volume of Ag particles their amount is comparable with the amount of Ag_2S particles.

The produced Ag_2S/Ag heteronanostructures combine ionic and electronic conductors. The heterostructures of this type containing Ag and Ag_2S nanofibers or a silver film with Ag_2S nanoclusters are considered as a potential basis for creating biosensors [31], resistive switches and nonvolatile memory devices [4-6,32]. The resistive switches consist of a superionic conductor located between two metal electrodes. In the case of Ag_2S/Ag heterostructures, one of the electrodes is silver, and the second electrode can be such metals as Pt, Au, and Cu.

In this study, Ag_2S/Ag heterostructures formed by Ag_2S and Ag nanoparticles have been produced by a simple method of hydrochemical bath deposition. Deposition of Ag_2S/Ag heterostructures on a substrate coated with a thin conducting metallic layer will make it possible to form a structure, which can work as a resistive switch. The action of the switch is based on the phase transformation of nonconducting α-Ag_2S acanthite into β-Ag_2S argentite exhibiting superionic conduction. The transition into a high-conduction state is due to abrupt disordering of the cationic sublattice.

In studies [33, 34] it was shown that a high-conduction state of a crystal can be achieved by electric field induced "melting" of the cationic sublattice taking place without heating of the crystal. Such transformation occurring as a result of applied external electric field was confirmed by the authors [4-6] with respect to nanocrystalline silver sulfide. The effect of external electric field induced abrupt disordering allows the realization of the superionic state of silver sulfide at room temperature. This opens up the possibilities for practical use of materials based on silver sulfide. Earlier we performed an *in situ* high-temperature scanning electron microscopy study of acanthite - argentite phase transformation during electron beam heating [21] and an *in situ* high-temperature XRD study of this transformation [23].

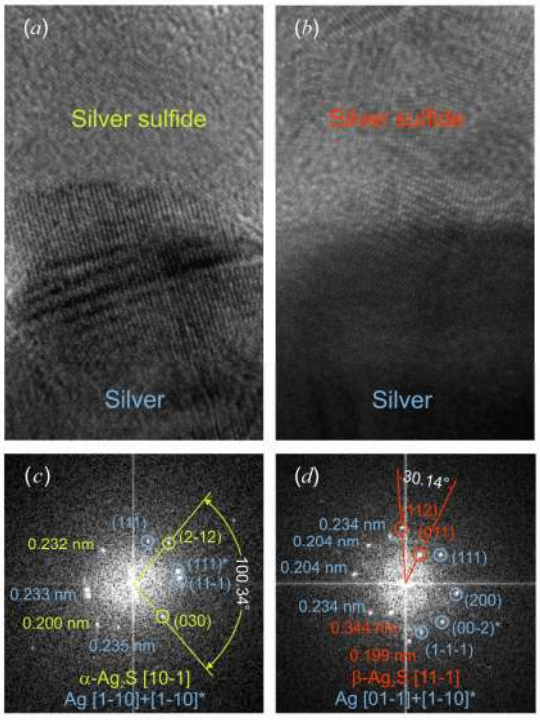

Figure 7. HRTEM images of region of transition between Ag and Ag_2S for off-state (*a*) and on-state (*b*) of Ag_2S/Ag heteronanostructure. The on-state arises as a result of applied external positive bias voltage to this Ag_2S/Ag heteronanostructure. The Pt electrode is located on the top part of the image, and Ag electrode is in the bottom part. Diffraction patterns (*c*) and (*d*) are obtained by FFT of HRTEM images (*a*) and (*b*), respectively. When Ag_2S/Ag heteronanostructure is transformed from the off-state into the on-state, along with Ag spots, the (011) and (112) spots of β-Ag_2S argentite appear on the diffraction pattern (*d*) instead of acanthite spots.

As already noted, the action of the resistive switch is based on the phase transformation of nonconducting α-Ag_2S acanthite

into superionic β-Ag_2S argentite. This phase transformation in Ag_2S/Ag heteronanostructure can be induced by external electric field without any heating.

We have studied preliminarily the switching processes in Ag_2S/Ag heteronanostructure. For this purpose, a metallic Pt microcontact was supplied to Ag_2S/Ag heteronanostructure and bias voltage was impressed so that Ag electrode was charged positively. When positive bias voltage increases to 500 mV, the conduction of the heteronanostructure grows and the nanodevice transforms into the on-state. The bias back to negative values decreases the conduction and the nanodevice transforms into the off-state.

Figure 7 displays a region of Ag_2S/Ag heteronanostructure where change of crystal structure at the transition from the off-state (Fig. 7*a*) to the on-state (Fig. 7*b*) can be observed. Using FFT of HRTEM images, we obtained the diffraction patterns (Fig. 7*c*, 7*d*). The diffraction pattern in Fig. 7*c* contains (111), (11-1) spots and twinning reflection (111)* corresponding to cubic (space group $Fm\bar{3}m$) silver, as well as (2-12) and (030) spots corresponding to monoclinic (space group $P2_1/c$) α-Ag_2S acanthite. The observed angle of 100. 3º between (2-12) and (030) spots of monoclinic acanthite coincides within measurement error with the theoretical value 100. 7º. The diffraction pattern (Fig. 7*d*) contains two sets of spots corresponding to two cubic phases. The (111), (200), (1-1-1) spots and the twinning spot (00-2)* correspond to cubic (space group $Fm\bar{3}m$) silver, and the (011) and (112) spots correspond to cubic (space group $Im\bar{3}m$) β-Ag_2S argentite. The observed angle of 30. 1º between the (011) and (112) spots of cubic β-Ag_2S argentite coincides with the theoretical value 30º. Experimental angles between diffraction spots of cubic silver (Fig. 7*c*, 7*d*) coincide with theoretical values. Thus, the applied bias really leads to the appearance of conducting β-Ag_2S argentite instead of nonconducting α-Ag_2S acanthite. The operation of a switch based on silver sulfide is schematically illustrated in Figure 8. The initial Ag_2S phase is a nonconducting acanthite α-Ag_2S (Fig. 8*a*). When a positive bias is applied, Ag^+ cations start to move toward the negatively charged cathode M and are reduced to Ag atoms during their transport. At the same time, the α-Ag_2S phase transforms into superionic β-Ag_2S argentite (Fig. 8*b*), and a continuous conductive channel is formed (Fig. 8*c*). The continuous conductive channel which is formed from argentite β-Ag_2S and silver Ag is retained, when the external field is turned off. This phenomenon can be considered as a memory effect (Fig. 8*c*). If a negative (reverse) bias is applied to the switch, the Ag nanocrystals start dissolving in argentite, the Ag^+ cations move to the anode, argentite transforms into the initial acanthite again, and the conductive channel breaks down (Fig. 8*d*).

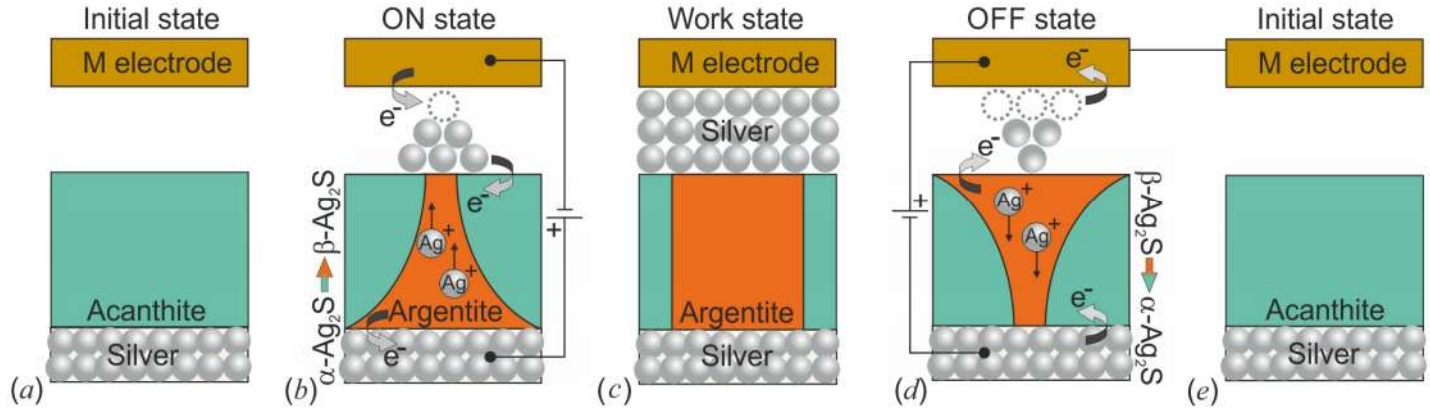

Figure 8. Scheme of the operation of an Ag_2S/Ag-based switch: (*a*) initial nonconducting state, (*b*) the appearance of a conductive channel upon the application of an external electric field that induces the transformation of acanthite α-Ag_2S into argentite β-Ag_2S, (*c*) a continuous conductive channel, (*d*) break down of the conductive channel upon the application of negative bias and the transition of argentite into initial acanthite, and (*e*) the disappearance of the conductive channel and turning-off of the switch.

Because of the formation of nonconducting acanthite, the conductive channel disappears, the switch transforms into the initial state and is turned off (Fig. 8*e*). If positive bias is applied once again, the destroyed conductive channel is restored due to the appearance of argentite and the formation of silver. According to [3, 6], the bias voltage which is sufficient to turn on and off the switch is in range from ±0. 2 to ±10. 0 V depending on the metal M used as the second electrode.

Ag_2S/Ag nanocomposites can be applied as promising biosensing probes. It is known that silver nanoparticles can be used as biosensors owing to their unique surface plasmon resonance, which depends on the size and shape of particles [31, 35]. However, Ag nanoparticles are easily oxidized; that is why they should be protected. The combination of Ag nanoparticles and chemically stable silver sulfide Ag_2S allows one to increase the stability of Ag nanoparticles and to use Ag_2S/Ag nanocomposites and Ag@Ag_2S core-shell structures for biosensing applications in the future. According to [36, 37], Ag_2S/Ag heteronanostructures possess considerable antibacterial activity and can be used in biology and medicine.

4. CONCLUSIONS

The Ag_2S/Ag heteronanostructures are formed in aqueous solutions of $AgNO_3$, Na_2S, and Na_3Cit with decreased concentration of sodium sulfide during synthesis in the light. The appearance of Ag nanoparticles is due to photochemical reduction of some Ag^+ ions by citrate ions. The produced Ag_2S/Ag heteronanostructures combine ionic and electronic conductors. A

high-conducting state of such heteronanostructure can be induced by external electric field without heating of this composite owing to phase transformation of nonconducting acanthite into argentite exhibiting superionic conduction. The argentite α-Ag_2S which appears as a result of the phase transformation and metallic silver Ag together form the conducting channel. The scheme of the operation of a resistive switch based on an Ag_2S/Ag heteronanostructure is proposed.

The main application of Ag_2S/Ag heteronanostructure is a creation of resistive switches and nonvolatile memory devices.

5. REFERENCES

[1] Faraday M., Experimental researches in electricity. - Fourth series, *Phil. Trans. Royal Soc. London*, 123, Art. 433-438, 507-522, **1833**.

[2] Faraday M., Experimental researches in electricity. - Twelfth series, *Phil. Trans. Royal Soc. London*, 128, Art. 1340, 83-123, **1838**.

[3] Liang C. H., Terabe K., Hasegawa T., Aono M., Resistance switching of an individual Ag_2S/Ag nanowire heterostructure, *Nanotechnology*, 18, 48, paper 485202 (5 pp.), **2007**.

[4] Xu Z., Bando Y., Wang W., Bai X., Golberg D., Real-time *in situ* HRTEM-resolved resistance switching of Ag_2S nanoscale ionic conductor, *ACS Nano*, 4, 5, 2515-2522, **2010**.

[5] Wang D., Liu L., Kim Y., Huang Z., Pantel D., Hesse D., Alexe M., Fabrication and characterization of extended arrays of Ag_2S/Ag nanodot resistive switches, *Appl. Phys. Lett.,* 98, 24, paper 243109 (3 pp.), **2011.**

[6] Belov A. N., Pyatilova O. V., Vorobiev M. I., Synthesis of Ag/Ag_2S nanoclusters resistive switches for memory cells, *Advanc. Nanoparticles*, 3, 1-4, **2014**.

[7] Sharma R. S., Chang Y. A., The Ag-S (silver-sulfur) system, *Bull. Alloy Phase Diagrams*, 7, 3, 263-269, **1986**.

[8] Pang M. L., Hu J. Y., Zeng H. C., Synthesis, morphological control, and antibacterial properties of hollow/solid Ag_2S/Ag heterodimers, *J. Am. Chem. Soc.,* 132, 31, 10771-10785, **2010**.

[9] Yang J., Ying J. Y., Nanocomposites of Ag_2S and noble metals, Angew. *Chem. Int. Ed.,* 50, 20, 4637-4643, **2011**.

[10] Pacholski C., Kornowski A., Weller H., Site-specific photodeposition of silver on ZnO nanorods, *Angew. Chem. Int. Ed.,* 43, 36, 4774-4777, **2004**.

[11] Fan F. -R., Ding Y., Liu D. -Y., Tian Z. -Q., Wang Z. L., Facet-selective epitaxial growth of heterogeneous nanostructures of semiconductor and metal: ZnO nanorods on Ag nanocrystals, J. *Am. Chem. Soc.* . 131, 34, 12036-12037, **2009**.

[12] Yang J., Ying J. Y., Room-temperature synthesis of nanocrystalline Ag_2S and its nanocomposites with gold, *Chem. Commun.,* 14, 22, 3187-3189, **2009**.

[13] Zhang W., Zhang L., Hui Z., Zhang X., Qian Y., Synthesis of nanocrystalline Ag_2S in aqueous solution, *Sol. State Ionics*, 130, 1-2, 111-114, **2000**.

[14] Pawar S. M., Pawar B. S., Kim J. H., Joo O. -S., Lokhande C. D., Recent status of chemical bath deposited metal chalcogenide and metal oxide thin films, *Curr. Appl. Phys.,* 11, 3, 117-161, **2011**.

[15] Sadovnikov S. I., Gusev A. I., Chemical deposition of nanocrystalline lead sulfide powders with controllable particle size, *J. Alloys Comp.,* 586, 105-112, **2014**.

[16] Sadovnikov S. I., Gusev A. I., Rempel A. A., Artificial silver sulfide Ag_2S: crystal structure and particle size in deposited powders, *Superlatt. Microstr.,* 83, 35-47, **2015**.

[17] Sadovnikov S. I., Rempel A. A., Synthesis of nanocrystalline silver sulfide, *Inorg. Mater.,* 51, 8, 759-766, **2015**.

[18] Zhu G. X., Xu Z., Controllable growth of semiconductor heterostructures mediated by bifunctional Ag_2S nanocrystals as catalyst or source-host, *J. Am. Chem. Soc.,* 133, 1, 148-157, **2011**.

[19] Sadovnikov S. I., Gusev A. I., Rempel A. A., Nonstoichiometry of nanocrystalline monoclinic silver sulfide, *Phys. Chem. Chem. Phys.,* 17, 19, 12466-12471, **2015**.

[20] Sadovnikov S. I., Gusev A. I., Gerasimov E. Yu., Rempel A. A., Facile synthesis of Ag_2S nanoparticles functionalized by carbon-containing citrate shell, *Chem. Phys. Lett.,* 642, 17-21, **2015**.

[21] Sadovnikov S. I., Gusev A. I., Rempel A. A., An *in situ* high-temperature scanning electron microscopy study of acanthite–argentite phase transformation in nanocrystalline silver sulfide powder, *Phys. Chem. Chem. Phys.,* 17, 32, 20495-20501, **2015**.

[22] Sadovnikov S. I., Gusev A. I., Rempel A. A., Nanocrystalline silver sulfide Ag_2S, *Rev Adv. Mater. Sci.,* 41, 1, 7-19, **2015**.

[23] Sadovnikov S. I., Gusev A. I., Chukin A. V., Rempel A. A., High-temperature X-ray diffraction and thermal expansion of nanocrystalline and coarse-crystalline acanthite α-Ag_2S and argentite β-Ag_2S, *Phys. Chem. Chem. Phys*., 18, 6, 4617-4626, **2016**.

[24] X'Pert HighScore Plus. Version 2. 2e (2. 2. 5). © 2009 PANalytical B. V. Almedo, the Netherlands.

[25] Gusev A. I., Rempel A. A., *Nanocrystalline Materials*, Cambridge Intern. Science Publ., Cambridge, **2004**.

[26] Gatan Misroscopy Suite. Gatan Inc Version 2. 31. 734. 0.

[27] http://www. gatan. com.

[28] Horvath B., Kawakita J., Chikyow T., Diffusion barrier and adhesion properties of SiO_xN_y and SiO_x layers between Ag/polypyrrole composites and Si substrates, *ACS Appl. Mat. Interf.,* 6, 12, 9201-9206 **2014**.

[29] Frueh A. J., The crystallography of silver sulfide, Ag_2S. *Zeitschr. Kristallographie*, 110, 1, 136-144, **1958**.

[30] Sadanaga R., Sueno S., X-ray study on the α-β transition of Ag_2S, *Mineralog. J. Japan.,* 5, 2, 124-148, **1967**.

[31] Liu B., Ma Z., Synthesis of Ag_2S-Ag nanoprisms and their use as DNA hybridization probes, *Small*, 7, 11, 1587-1592, **2011**.

[32] Terabe K., Hasegawa T., Nakayama T., Aono M., Quantized Conductance Atomic Switch, *Nature*, 433, 7021, 47-50, **2005**.

[33] Kharkats Yu. I., Electric-field induced transition to superionic conductive state, *Fiz. Tverd. Tela*, 23, 7, 2190-2192, **1981**. (*in Russian*).

[34] Gurevich Yu. Ya., Kharkats Yu. I., Features of the thermodynamics of superionic conductors, *Sov. Phys. Uspekhi*, 25, 4, 257-276, **1982**.

[35] Hu M., Chen J. Y., Li Z. Y., Au L., Hartland G. V., Li X. D., Marquez M., Xia Y. N,. Gold nanostructures: engineering their plasmonic properties for biomedical applications. *Chem. Soc. Rev*., 35, 11, 1084-1094, **2006**.

[36] Ma X., Zhao Y., Jiang X., Liu W., Liu S., Tang Z., Facile preparation of Ag_2S/Ag semiconductor/metal heteronanostructures with remarkable antibacterial properties, *ChemPhysChem*, 13, 10, 2531-2535, **2012**.

[37] Sadovnikov S. I., Kuznetsova Yu. V., Rempel A. A., Ag_2S silver sulfide nanoparticles and colloidal solutions: Synthesis and properties, *Nanostruct. Nano-Objects*, 7, 81-91, **2016**.

6. ACKNOWLEDGEMENTS

This work is financially supported by the Russian Science Foundation (Grant 14-23-00025) through the Institute of Solid State Chemistry of the Ural Branch of the RAS. Authors are grateful to Dr. E. Yu. Gerasimov for the help in electron microscopy study.

© 2016 by the authors. This article is an open access article distributed under the terms and conditions of the Creative Commons Attribution license (http://creativecommons. org/licenses/by/4. 0/).